NASA Technical Paper 1333

Atmospheric Entry and Fragmentation of Dense Meteoroids

T. Dale Bess

JANUARY 1979

NASA

NASA Technical Paper 1333

Atmospheric Entry and Fragmentation of Dense Meteoroids

T. Dale Bess
Langley Research Center
Hampton, Virginia

National Aeronautics
and Space Administration

**Scientific and Technical
Information Office**

1979

SUMMARY

Fragmentation characteristics for four artificial meteoroids of high density and high tensile strength with varying size, velocity, and material are investigated. The meteoroids analyzed were lifted to natural meteor altitude by a rocket vehicle system. The meteoroids were then accelerated back into the Earth's atmosphere at natural meteor velocities.

Studies of natural meteors have indicated that anomalous deceleration in these meteors is caused by progressive fragmentation. However, the meteoroids were generally assumed to be porous and of weak structure. The fact that high-density and high tensile strength meteoroids might have anomalous deceleration due to fragmentation was not seriously considered.

The present study addresses anomalous deceleration of high-density meteoroids. The analysis is based on forcing the theoretical meteor deceleration curve to match its corresponding measured deceleration curve by allowing the meteoroid to fragment in a specified manner. Best results were obtained from a fragmentation model based on a geometrical progression of breakup along the meteor trail.

INTRODUCTION

The meteoroids that produce faint photographic meteors are usually visualized as having a very porous and fragile structure with a low tensile strength (ref. 1). Anomalies in the deceleration of these faint meteors is a common occurrence as ascertained from observational data on natural meteors. These anomalies are the progressive departure of observed decelerations of natural meteors from the deceleration expected on the basis of single-body meteor theory. These anomalies also show up in the meteor light curve in that faint meteors mostly rise to maximum brightness faster and have a shorter duration than prescribed by the theory based on single-body meteor ablation.

In reference 1 an explanation for the anomalous deceleration observed in faint meteors has been shown to be due to progressive fragmentation. Photographic meteor observations were used to derive empirical corrections which account for progressive fragmentation. The theory of reference 1 is based mostly on faint meteors and on the idea that these faint meteors are of porous and fragile structure. The fact that the meteoroids may have high density with high tensile strength has not been seriously considered.

The purpose of this paper is to analyze and report the results from four artificial meteoroids of high density and high tensile strength. These meteoroids were lifted to natural meteor heights by using a rocket vehicle system and entered the atmosphere at meteor speeds. The departure of observed deceleration of the four meteoroids from the deceleration expected on the basis of

single-body theory is investigated, and the resulting fragmentation characteristics are determined.

SYMBOLS

A	effective cross-sectional area of object, cm
a,b,c,k	constants used in least-squares solution of distance equation
D	distance along meteor trail, km
I	radiant power of point on meteor trail, J/sec
$I_{o,s}$	radiant power of zero magnitude meteor as detected by system s, J/sec
K	dimensionless meteoroid shape factor
l	characteristic dimension of meteoroid, diameter in cm
M	absolute meteor magnitude
m	instantaneous meteoroid mass, g
Δm_j	mass loss of meteoroid, g
R	Reynolds number
t	time, sec
V	meteoroid velocity, km/sec
V_T	mean thermal velocity of atoms evaporated from surface of meteoroid, km/sec
β	directionality coefficient of evaporation
Γ	drag coefficient of meteoroid
δ	meteoroid density, g/cm^3
ν	kinematic viscosity, km^2/sec
ρ	atmospheric density, g/cm^3
τ_o'	luminosity coefficient, $sec^4/g\text{-}cm^3$

Subscript:

j	amount of mass lost over short time increment

A dot over a symbol refers to the first derivative.

EXPERIMENT

Vehicle and Trajectory

The four artificial meteors analyzed were produced from rocket flights launched from NASA's Wallops Flight Center, Va. The experiments took place during a 6-year time period from 1962 to 1967. The primary objective of these experiments was to determine luminous efficiencies of artificial meteors.

Three of the experiments used the Trailblazer II rocket vehicle system. A detailed description of the Trailblazer II rocket vehicle can be found in references 2 to 5. A photograph of the Trailblazer II rocket vehicle is shown in figure 1. The vehicle has six stages and produces one artificial meteor. It has two booster stages and a velocity package that contains a single reentry system. This reentry system, shown in figure 2, consists of three rocket motors and an accelerator containing the artificial meteoroid material.

One experiment used the Nike-Cajun rocket vehicle system. A description of the Nike-Cajun rocket vehicle can be found in reference 6. The Nike-Cajun vehicle, shown in figure 3, has six stages and is designed to produce two artificial meteors separated in time. The rocket system consists of two rocket motors as booster stages and a velocity package, shown in figure 4, that contains two separate reentry systems. Each reentry system consists of a 12.7-cm spherical rocket motor and a shaped charge accelerator containing the artificial meteoroid material.

Discussions in following sections of this paper refer to these four experiments as meteor 1, meteor 2, meteor 3, and meteor 4. Data essential for analysis of the four meteors are given in table I.

Accelerators and Pellet

Two types of accelerators were used to produce the artificial meteors. Two of the Trailblazer II vehicles used air-cavity accelerators, as shown in figure 5, to accelerate an artificial meteoroid of ductile metal initially in the form of a disk. These air-cavity accelerators gave the artificial meteoroids a velocity increment of about 4.3 km/sec. At this velocity, the meteoroid could be recovered from ground test firings, and the mass could be accurately determined. Figure 6 is a photograph showing one of these artificial meteoroids before ground test firing and after recovery from test firing. A description of the air-cavity accelerator is given in references 7 and 8.

The other Trailblazer II experiment and the Nike-Cajun experiment used shaped charge accelerators, as shown in figure 7, to produce a small, irregularly shaped meteoroid with a velocity increment of about 9.5 km/sec. The projectile from this type of accelerator could not be recovered from ground test firings. The masses in this case had to be determined indirectly from measurements of flashed X-ray photographs. Figure 8 shows a flash radiograph of one of these meteoroids taken during ground test firings. A more detailed description of the shaped charge accelerator is given in references 9 and 10.

In all four experiments the maximum velocity of the meteoroid was the velocity increment due to the accelerator plus the velocity increment due to the rocket system connected in tandem with the accelerator.

Photographic Instrumentation

The luminous meteor trails produced by the four meteor experiments were photographed by ground-based ballistic cameras. The types used were the Super-Schmidt cameras, the BC-4 ballistic cameras, and modified K-24 and K-37 cameras. Optical characteristics of these cameras are given in reference 5. Camera sites were located at Wallops Flight Center, Va., Eastville, Va., Sandbridge, Va., and Coquina Beach, N.C. The locations of the four camera sites with respect to the reentry areas of the Trailblazer II and Nike-Cajun vehicles are shown in figure 9. Figure 10 shows meteor 1 photographed during atmospheric entry. The luminous trail from this meteoroid is similar in appearance to the luminous trails of the other three. Photographs of this type from two different locations are sufficient for determining the position of the meteor. If at least one photograph is taken by using a camera with repeating shutters, a chopped meteor trail results and velocity and deceleration of the meteor can be determined.

Light-intensity data of the meteor trail is furnished by these photographs and is sufficient to define the meteor light curve. The mass loss of the meteoroid as it passes through the atmosphere is proportional to the light intensity as determined from the light curve. A thorough description of photographic photometry for defining the meteor light curve is given in reference 11.

METHOD OF ANALYSIS

The objective of this analysis is to determine the fragmentation characteristics during atmospheric entry of high density and high tensile strength artificial meteoroids of known mass, shape, and velocity.

The approach uses theoretical equations of meteor physics for nonfragmenting meteoroids together with available measured data obtained from photographs of the luminous meteor trails. The analysis for determining fragmentation characteristics is based on comparing and fitting the theoretical velocity-altitude (deceleration) curve of a nonfragmenting meteoroid with the measured (observationally determined) deceleration curve of the same meteoroid. By integrating the meteoroid drag equation, which describes the motion of a nonfragmenting meteoroid entering the atmosphere, and then considering the meteoroid to fragment in different ways, a fit of theoretical and measured deceleration curves can be obtained. The standard assumption that mass loss, and thus the change in mass of the meteoroid along the trail, is proportional to the light intensity as determined from the measured light curve of the meteor entry is used. The basic meteor equations used in the analysis of the data are the theoretical drag equation and the equations for luminosity, mass loss, and measured velocity, hereafter referred to as the data-reduction equations.

Drag Equation

From reference 12 the drag or resistance equation for a meteoroid entering the atmosphere is

$$\frac{dV}{dt} = - \frac{\Gamma K \rho}{\delta^{2/3} m^{1/3}} V^2 + \frac{\beta V_T}{m} \frac{dm}{dt} \tag{1}$$

The directionality coefficient of evaporation β is 4/9 for hemispheric evaporation and 0 for isotropic evaporation.

Three parameters in equation (1), which are not accurately known for most natural meteoroids, are the drag coefficient Γ, the shape factor K, and the density of the meteoroid δ. The drag coefficient Γ and the shape factor K depend primarily upon the shape and orientation of the meteoroid. For most natural meteoroids Γ can vary from a low value of 0.5 to a high value of 1.0 and the shape factor K is assumed to be that for a sphere. Densities of the artificial meteoroids are known, and since their approximate shapes are known, drag coefficients and shape factors can be approximately determined.

The artificial meteoroids that formed meteor 1 and meteor 4 were approximately rod shaped before any fragmentation began. (See fig. 8.) Results of comparing theoretical and measured velocity curves showed that these meteoroids were initially oriented in a near streamline direction. A constant drag coefficient of 0.75 was used for these two meteoroids before fragmentation began. This value of 0.75 represents an average drag coefficient for a round leading edge $\left(C_{D_e} = 1.25\right)$ and a flat edge $\left(C_{D_e} = 1.75\right)$ (values of C_{D_e} from ref. 13, ch. 18) where

$$\Gamma = \frac{1}{2} C_{D_e} \tag{2}$$

and C_{D_e} is the frontal area of the body. After fragmentation of the meteoroids begins, all fragments are assumed to be spherical in shape, and the drag coefficient is given by (from ref. 13, ch. 19)

$$\Gamma = \frac{1}{2}\left(0.95 + \frac{5}{\sqrt{R}}\right) \tag{3}$$

In this equation R is the Reynolds number defined as

$$R \equiv \frac{Vl}{\nu} \tag{4}$$

The artificial meteoroids that formed meteor 2 and meteor 3 were approximately disk shaped before fragmentation began. (See fig. 6.) A drag coefficient determined from equation (3) was used for these meteoroids over their entire trajectory (ref. 13).

The dimensionless shape factor K from equation (1) is defined such that

$$K\left(\frac{m}{\delta}\right)^{2/3} \equiv A \tag{5}$$

For a sphere, $K = 1.21$. For a cylinder, $K > 1$ for the broadside aspect and $K < 1$ for the streamline aspect.

The second term in equation (1) is due to the reactive force of vaporizing meteoroid material and is greatest for large meteoroids where vaporization is limited to the front hemispherical surface. The four artificial meteoroids are small enough so that mean isotropic evaporation probably prevails and the reactive force term can be neglected.

Data-Reduction Equations

Reference 6 gives the relation for determining the meteor magnitude of a point on the meteor trail in terms of radiant power I. In terms of radiant power

$$M = -2.5 \log \frac{I}{I_{o,s}} \tag{6}$$

or

$$\frac{I}{I_{o,s}} = 10^{-0.4M} \tag{7}$$

The brightness in meteor magnitude along the optical meteor trail is the meteor light curve. The meteor light curve can be used to determine a time history of the meteoroid's mass loss.

The meteor magnitude in equations (6) and (7) is measured directly from photographs of the visible meteor trail. Magnitude is obtained by comparing points along the meteor trail with the star background for which magnitudes have been cataloged. Some corrections are necessary to arrive at the final value for magnitude. Details of the procedure for determining meteor magnitude and making the necessary corrections is given in reference 14. From reference 6 the relation between meteor luminosity and the time rate of mass loss

of the meteoroid, assuming a constant luminosity to mass-loss proportionality, is given by

$$\frac{I}{I_{o,s}} = 10^{-0.4m} = \frac{1}{2}\,\tau_o'\,\frac{\Delta m}{\Delta t}\,v^3 \tag{8}$$

The luminosity coefficient is assumed constant, and for small meteoroids the velocity is nearly constant during the ablation process. Thus, from equation (8) the amount of original meteoroid mass ablated away during a small time increment Δt_j of visible meteor trail is

$$\Delta m_j = 2 \times 10^{-0.4M_j}\,\frac{\Delta t_j}{\tau_o' v^3} \tag{9}$$

The original mass of the meteoroid is the sum of all Δm_j over the meteor trail, assuming that the meteoroid is completely consumed. In this case the original meteoroid mass is

$$m = 2\sum_{j=1}^{n} 10^{-0.4M_j}\,\frac{\Delta t_j}{\tau_o' v^3} \tag{10}$$

The ratio of Δm_j to m is therefore

$$\frac{\Delta m_j}{m} = \frac{2 \times 10^{-0.4M_j}\,\Delta t_j/\tau_o' v^3}{2\sum_{j=1}^{n} 10^{-0.4M_j}\,\Delta t_j/\tau_o' v^3} \tag{11}$$

For constant V and constant τ_o'

$$\frac{\Delta m_j}{m} = \frac{10^{-0.4M_j}}{\sum_{j=1}^{n} 10^{-0.4M_j}} \tag{12}$$

Equation (12) can be used to determine mass loss Δm_j over a short time increment. Since Δm_j can be determined, an instantaneous mass curve against either time or altitude can be determined for the meteoroid. This instantaneous mass is used in the theoretical drag equation but does not take into account the fact that mass at any time may be a cluster of small individual fragments, each of which acts like a separate meteoroid.

Measured velocity and deceleration along a meteor trail are determined from a purely empirical relation. (See refs. 14 and 15.) The distance along a chopped meteor trail and the associated relative time, as determined from timed shutter breaker from a ballistic camera, are given by

$$D = a + bt + ce^{kt} \tag{13}$$

where a, b, c, and k are constants to be determined. Velocities and decelerations are easily obtained by differentiation; thus

$$V = \frac{dD}{dt} = b + kce^{kt} \tag{14}$$

$$\dot{V} = \frac{dV}{dt} = k^2ce^{kt} \tag{15}$$

The probable error for the initial meteor velocity appears to be on the order of 0.01 percent for good natural meteor trails. For some natural meteor trails with poor initial velocity determinations, the probable error is about 0.3 percent. The probable error for the constant c is on the order of 3 percent. At the end of the visible meteor trail the initial meteor velocity has usually been reduced by about 10 percent. For a 10-km/sec meteor, the velocity has been reduced by about 1 km/sec. This reduction is accounted for in the second term of equation (14). Three percent of this reduction can be attributed to the probable error in c. Combining the errors for the initial velocity and the probable error in the constant c, a total error in measured velocity of about 0.05 km/sec may be expected.

RESULTS AND DISCUSSION

Data from the four artificial meteoroids were analyzed to determine fragmentation characteristics. These characteristics were determined by comparing the theoretical deceleration curves of the meteoroids with their measured deceleration curves.

Light-intensity curves for the four artificial meteors are shown in figure 11. Absolute magnitude of each meteor is plotted against its altitude in kilometers. Meteor 1 and meteor 3 have pronounced irregularities in their light curves. Classical meteor theory predicts the rate of ablation of each meteoroid to be proportional to meteor luminosity. The meteor luminosity can be determined from the meteor light curve.

By taking absolute magnitude data from the light-intensity curves and using equation (10), curves of instantaneous meteoroid mass as a function of meteor altitude can be determined. The results for the four meteoroids are presented in figure 12. The curves in figure 12 represent polynomial fits to the data. Instantaneous mass values from figure 12 are used in equation (1) when calculating theoretical velocities of the ablating meteoroids.

By comparing the theoretical and measured deceleration curves, the fragmentation characteristics of the four meteoroids can be determined. Figure 13 shows theoretical deceleration curves for the four meteoroids which are ablating but assumed not to be fragmenting. These curves are superimposed on the measured deceleration curves of the same four meteoroids. A study of figure 13

shows that, for each of the four meteoroids, theoretical and measured deceleration curves agree well during the early time history of the trajectory. However, theoretical and measured curves begin to differ near the end of the meteor trail. Natural meteor deceleration time histories show the same behavior. Results of computations for each of the four artificial meteoroids show that varying the dimensionless shape factor K or the dimensionless drag coefficient Γ cannot account for the drastic change in deceleration. Meteoroid fragmentation is an apparent explanation for the anomalous change in deceleration. Visible observational evidence supporting this hypothesis are the irregularities in the measured light curves.

A primary part of the present analysis is to match the theoretical deceleration history determined from equation (1) with the measured deceleration history determined from equation (14). In order to obtain a match of the theoretical and measured deceleration curves, each of the four meteoroids being analyzed is considered to break up (geometrically) into specified numbers of fragments of equal mass at specified altitudes. Each fragment then behaves like a separate meteoroid of smaller mass with its velocity again described by equation (1). Figure 14 shows the comparison of theoretical velocity-altitude curves for the four meteoroids, taking this form of fragmentation into account. The best matches of measured and theoretical decelerations were obtained by using a simple geometrical progression to describe meteoroid fragmentation. When fragmentation begins to occur, each fragment then acts like a single meteoroid, which is described by single-body theory until it again fragments.

Meteor 1 was a 0.88-g nickel meteoroid with an initial velocity of 11.38 km/sec. This meteoroid was considered to fragment into two pieces at an altitude of 74.5 km, that is, that point at which the deceleration curve for the nonfragmenting meteoroid first deviates from the measured deceleration curve. At each 0.5-km interval thereafter each fragment is considered to break into two pieces of equal mass until a total of 64 fragments exists at an altitude of 72 km. At 71.4-km altitude where a significant increase in luminosity occurs, each fragment is considered to break up again into a specified number x of fragments. A number of deceleration curves for different values of x are shown for meteor 1. One curve is for a meteoroid that breaks into 64 fragments, that is, no further breakup when anomaly occurred in light curve. Other curves represent deceleration of a meteoroid that breaks into a total of 128 and 256 fragments at 71.4 km. A comparison of the computed deceleration curves for meteor 1 with its measured deceleration curve shows that fewer than 256 fragments may have existed immediately after the anomaly in the light curve occurred. The 128-fragment curve agrees with the measured curve until about 70 km. These curves indicate that the breakup was progressive even after the anomaly occurred.

Meteor 2 was a large, 5.7-g steel meteoroid with an initial velocity of 10.93 km/sec. This meteoroid was considered to fragment into two pieces at an altitude of 67 km. At each 0.5 km thereafter each fragment was allowed to break into two pieces until a total of 32 fragments existed at an altitude of 65 km. No anomaly occurred in this meteor. The resulting deceleration curve matches the measured deceleration very well.

Meteor 3 was a 2.2-g steel meteoroid with an initial velocity of 11.91 km/sec. The theoretical and measured deceleration curves began to differ at a height of about 71.5 km. At this point the meteoroid breakup was considered to begin. Breakup into 2, 4, 8, 16, and 32 fragments occurred at 0.5-km intervals. At an altitude of about 69 km an anomaly occurred, thereby causing an increase in meteor luminosity. At the point of the anomaly each fragment is considered to break up into a specified number of fragments. A number of deceleration curves are shown for meteor 3. One curve represents meteoroid breakup into a total of 64 fragments; other curves represent 128 and 256 fragments. A comparison of the computed deceleration curves for meteor 3 with its measured deceleration curve shows that more than 32 fragments may have existed at the time of the anomaly in the light curve because the theoretical velocity is still larger than the measured velocity.

Meteor 4 was a 0.81-g iron meteoroid with an initial velocity of 16.43 km/sec. No anomalies were apparent in the light curve. The theoretical and measured deceleration curve began to differ at an altitude of about 80 km. At this point the progressive meteoroid breakup was considered to begin. Two curves are shown. One curve represents breakup into 2, 4, 8, 16, 32, 64, and 128 fragments at 0.5-km intervals. The other curve represents breakup into 2, 4, 8, 16, 32, 64, 128, and 256 fragments at 0.5-km intervals. The measured deceleration curve is bounded by these two curves.

The computed deceleration curves in figure 14 thus compare favorably with their measured deceleration curves even though the model is based on a simple geometric progression of meteoroid breakup into fragments of equal masses. In reality the meteoroids, although undergoing progressive fragmentation, break up into a number of fragments of unequal masses. Furthermore, even before meteoroid breakup begins, appreciable ablation has occurred as ascertained from mass-loss curves for the four meteoroids in figure 12. The mass loss before fragmentation, calculated from equation (12), ranges from 12 percent in meteor 1 to about 51 percent in meteor 4. These mass losses are due to either or both of the following processes: Direct vaporization from the meteoroid surface; flaking of very small particles from the meteoroid surface which then vaporize. Particles due to flaking are on the order of 10^{-5} to 10^{-6} g (ref. 16). As long as direct vaporization and flaking of small particles are the mode of ablation, single-body theory will describe the meteoroid's deceleration; however, when the meteoroid begins to break up, single-body theory is no longer valid and a modified theory that combines single-body theory and progressive fragmentation must be used.

In reference 17 an investigation was made of the thermal stresses in iron and stone meteoroids during both preheating and ablation stages. The model is based on a spherical meteoroid. This investigation shows that meteoroid fragmentation due to thermal shock is size dependent, and that during the ablation stage meteoroid fracturing is not expected for large meteoroids but is restricted to bodies less than 10 cm in radius. Based on the results from reference 17, the cause of fragmentation present in the four meteoroids considered in this study may be due to thermal stresses from unequal meteoroid heating.

CONCLUDING REMARKS

Anomalies in the deceleration of faint optical meteors have been interpreted as being due to progressive fragmentation caused by porous and fragile meteoroid material of low tensile strength. The analysis in the present paper indicates that the same type of deceleration behavior exists for small mass, high density, and high tensile strength material entering the atmosphere at low meteor velocities. From this analysis, which indicates significant progressive fragmentation and which is consistent with observed faster rise to maximum brightness and shorter duration light curves, the interpretation of the faint meteor anomaly, indicating low density and fragile structure, should be reexamined.

Langley Research Center
National Aeronautics and Space Administration
Hampton, VA 23665
November 8, 1978

REFERENCES

1. Jacchia, Luigi G.: The Physical Theory of Meteors. VIII. Fragmentation as Cause of the Faint-Meteor Anomaly. Astrophys. J., vol. 121, no. 2, Mar. 1955, pp. 521-527.

2. Lunstrom, Reginald R.; Henning, Allen B.; and Hook, W. Ray: Description and Performance of Three Trailblazer II Reentry Research Vehicles. NASA TN D-1866, 1964.

3. Ayers, Wendell G.: Luminous Efficiency of an Artificial Meteor at 11.9 Kilometers Per Second. NASA TN D-2931, 1965.

4. Robertson, J. B.; and Ayers, Wendell G.: Photometry of an Iron Artificial Meteor Reentering at 11 Kilometers Per Second. NASA TN D-4312, 1968.

5. Ayers, W. G.; McCrosky, R. E.; and Shao, C.-Y.: Photographic Observations of 10 Artificial Meteors. Spec. Rep. No. 317, Smithsonian Inst. Astrophys. Obs., June 5, 1970.

6. Bess, T. Dale: Luminous Efficiencies of Three Nickel Artificial Meteors Between 9.8 and 11.4 Kilometer Per Second. NASA TN D-4666, 1968.

7. Kineke, John H., Jr.; and Holloway, Lee S.: Macro-Pellet Projection With an Air Cavity High Explosive Charge for Impact Studies. Memo. Rep. No. 1264, Ballistic Res. Labs., Aberdeen Proving Ground, Apr. 1960.

8. Kineke, John H., Jr.; and West, Carroll E., Jr.: An Improved Air-Cavity Explosive Charge for Accelerating Steel and Nickel Pellets. Memo. Rep. No. 1783, Ballistic Res. Labs., Aberdeen Proving Ground, Jan. 1967.

9. Woodall, R. L.; and Clark, E. L.: Development and Testing of Advanced Shaped Charge Meteoritic Simulators. Part II - Calibration of Flight Guns. NASA CR-66216, Firestone Tire & Rubber Co., 1966.

10. Clark, E.: Development and Testing of Shaped Charge Meteoritic Simulators - Calibration Study. Contract NAS1-4187, Firestone Tire & Rubber Co., Oct. 1965.

11. Ayers, Wendell G.: Photographic Photometry of Artificial Meteors. NASA TN D-4667, 1968.

12. Varob'eva, V. A.; and Kramer, E. N.: Deceleration of Meteoric Objects in the Visible Part of the Trajectory. Sol. Syst. Res. (Engl. Transl.), vol. 6, no. 1, Jan.-Mar. 1972, pp. 24-29.

13. Hoerner, Sighard F.: Fluid-Dynamic Drag. Hoerner Fluid Dynamics (Brick Town, N.J.), c.1965.

14. Whipple, Fred L.; and Jacchia, Luigi G.: Reduction Methods for Photographic Meteor Trails. Smithsonian Contrib. Astrophys., vol. 1, no. 2, 1957, pp. 183-206.

15. Jacchia, Luigi G.; and Whipple, Fred L.: Precision Orbits of 413 Photographic Meteors. Smithsonian Contrib. Astrophys., vol. 4, no. 4, 1961, pp. 97-129.

16. McCrosky, Richard E.: The Meteor Wake. Astron. J., Mar. 1958, pp. 97-106.

17. McCrosky, Richard E.; and Ceplecha, Zdenek: Fireballs and the Physical Theory of Meteors. Spec. Rep. No. 305, Smithsonian Astrophys. Obs., Nov. 1969.

TABLE I.- EXPERIMENTAL DATA FOR FOUR ARTIFICIAL METEORS

Meteor	Date	Vehicle	Accelerator	Material	Initial mass, g (*)	Initial velocity, km/sec
1	Sept. 17, 1966	Nike-Cajun	Shaped charge	Nickel	0.88	11.38
2	Mar. 17, 1966	Trailblazer II	Air cavity	1020 steel	5.7	10.93
3	May 6, 1962	Trailblazer II	Air cavity	Stainless steel	2.2	11.91
4	Feb. 14, 1967	Trailblazer II	Shaped charge	Iron	.81	16.43

*Estimated from ground measurements.

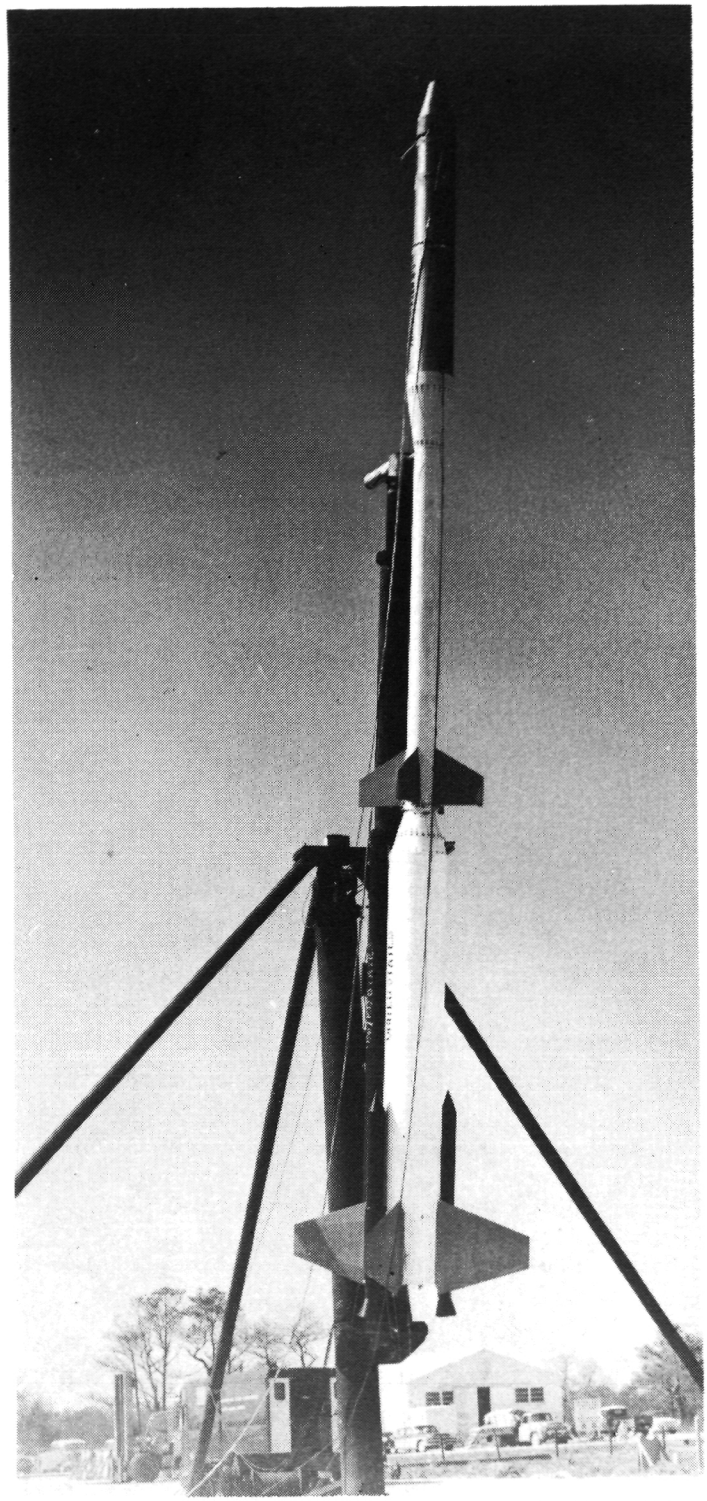

L-62-4432.1

Figure 1.- Trailblazer II in launch position.

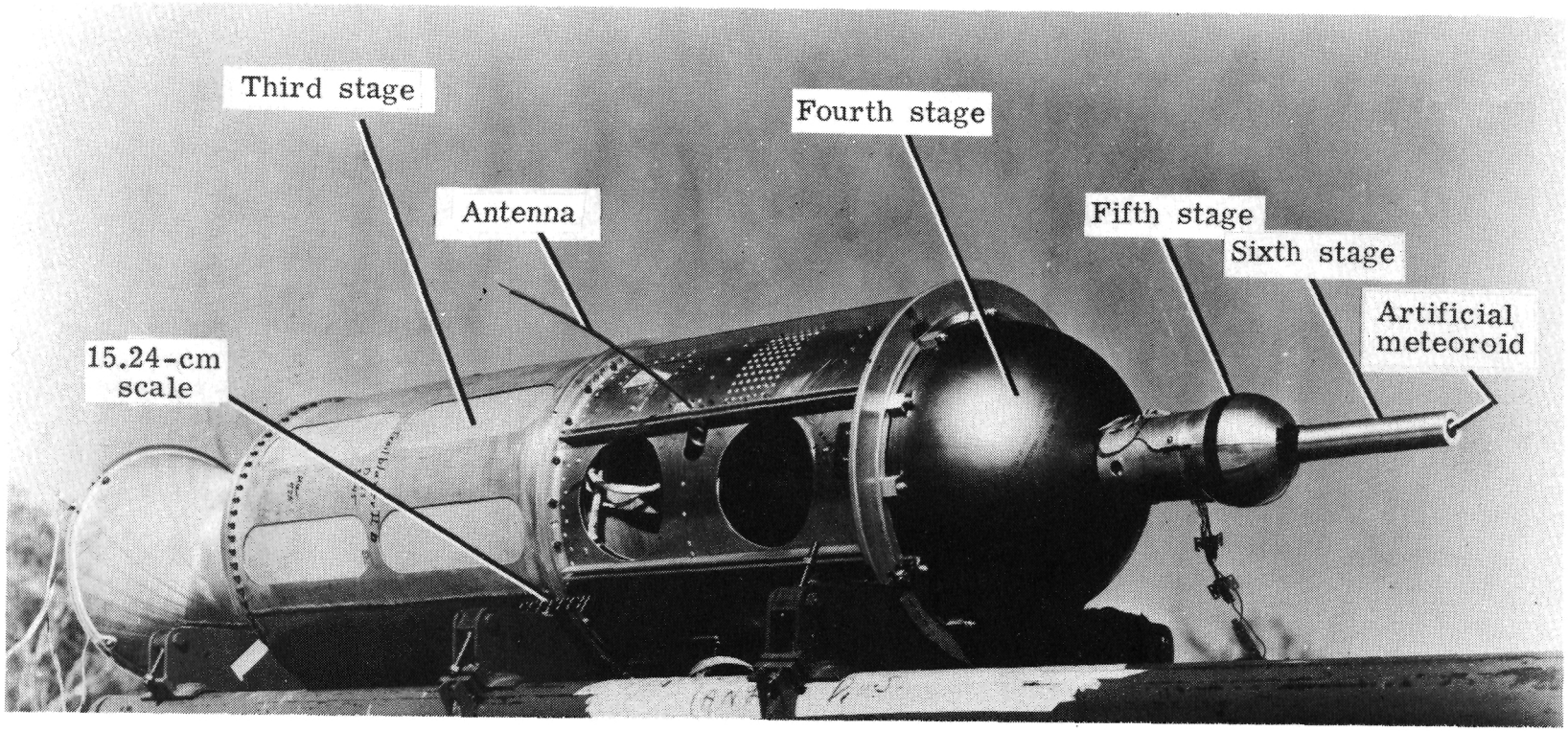

L-62-4040.2

Figure 2.- Reentry stages of Trailblazer II.

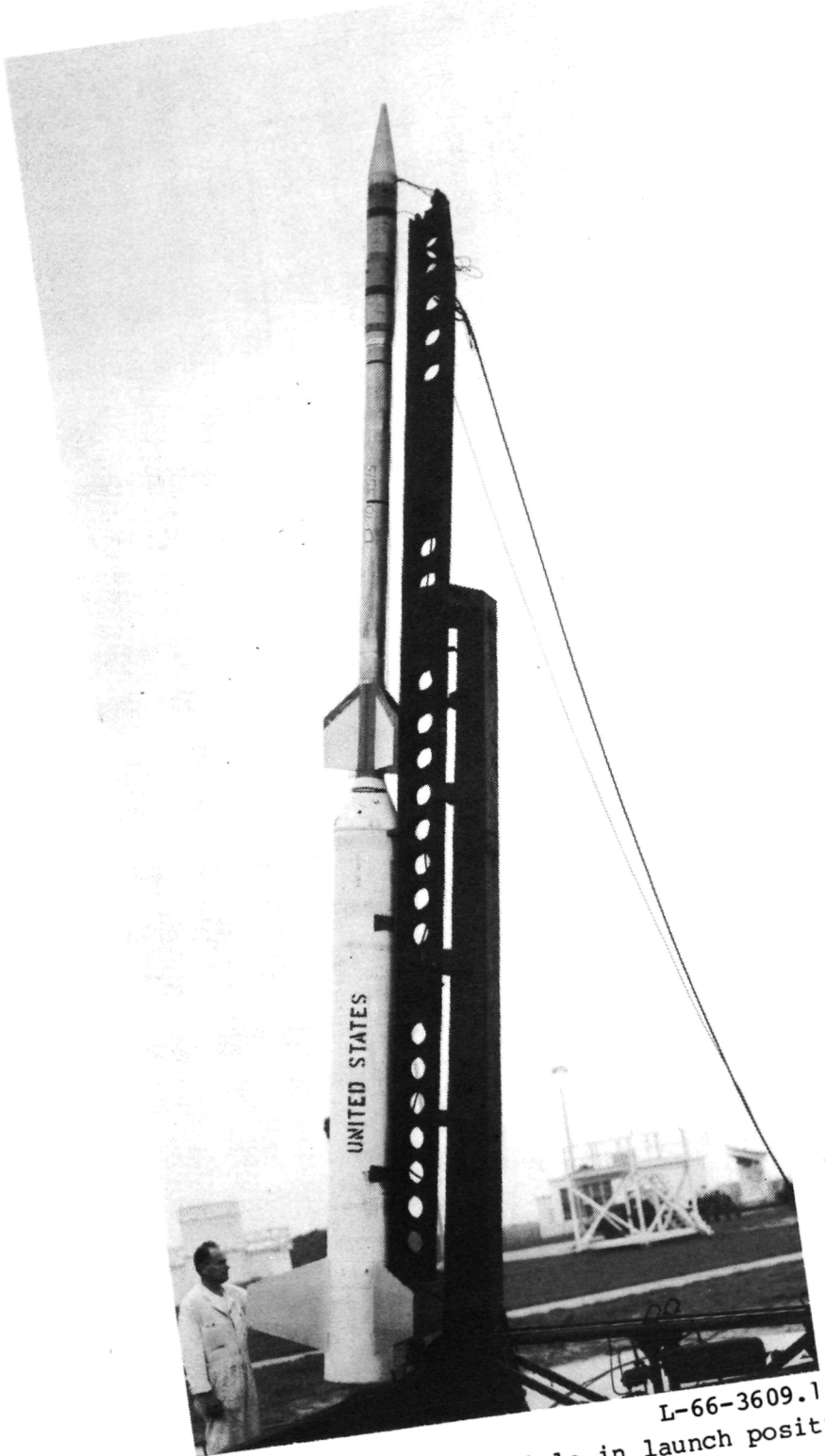

L-66-3609.1

Figure 3.- Nike-Cajun vehicle in launch position.

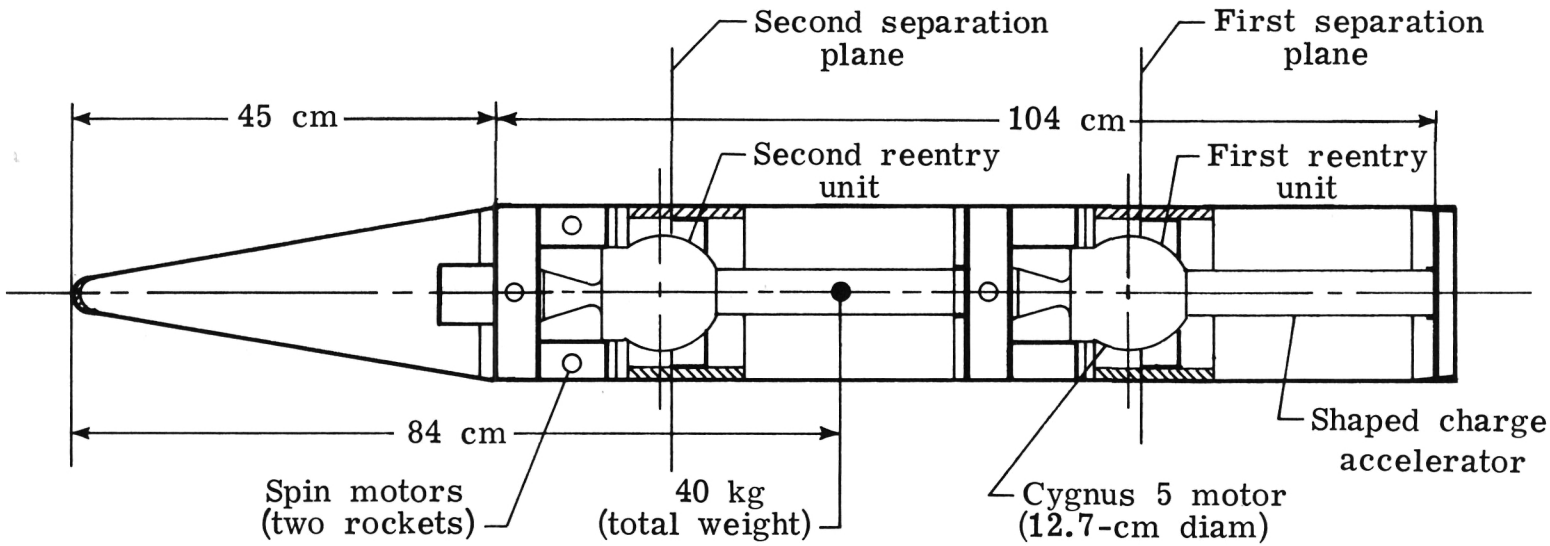

Figure 4.- Sketch of Nike-Cajun velocity package showing reentry stages.

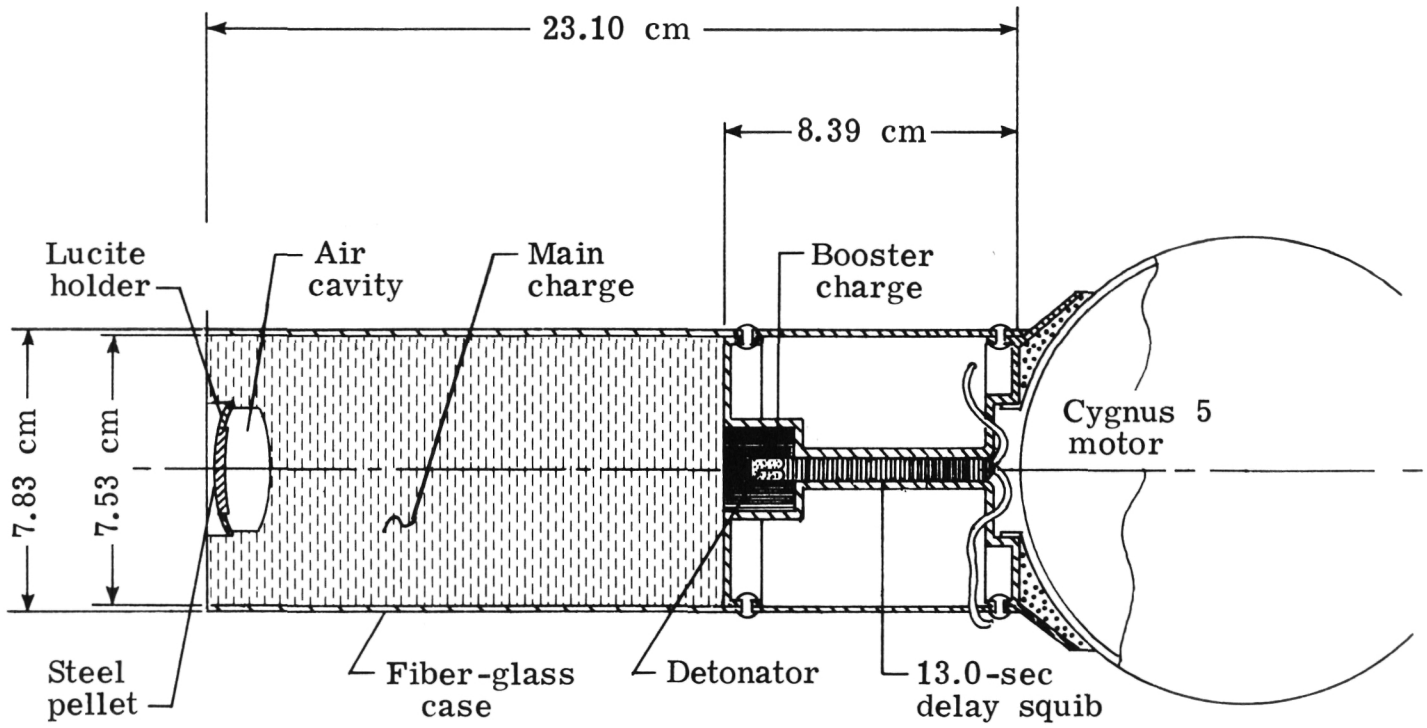

Figure 5.- Explosive accelerator (air-cavity gun).

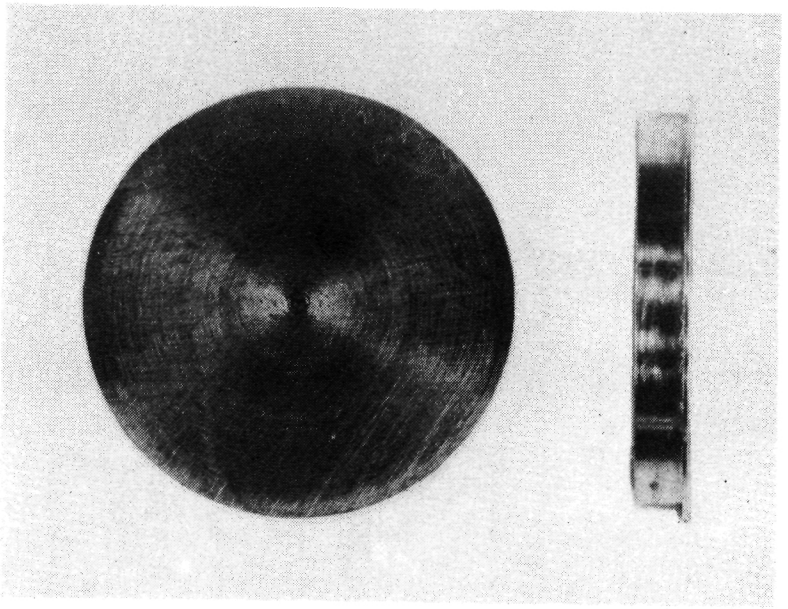

(a) Projectile before ground firing of air-cavity gun.

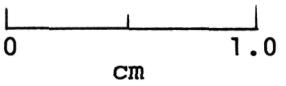

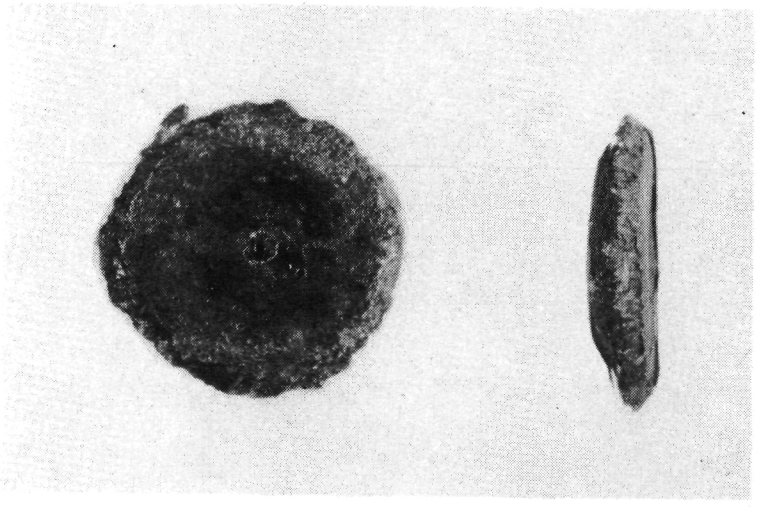

(b) Projectile recovered from ground firing of air-cavity gun.

L-78-156

Figure 6.- Projectile from air-cavity guns.

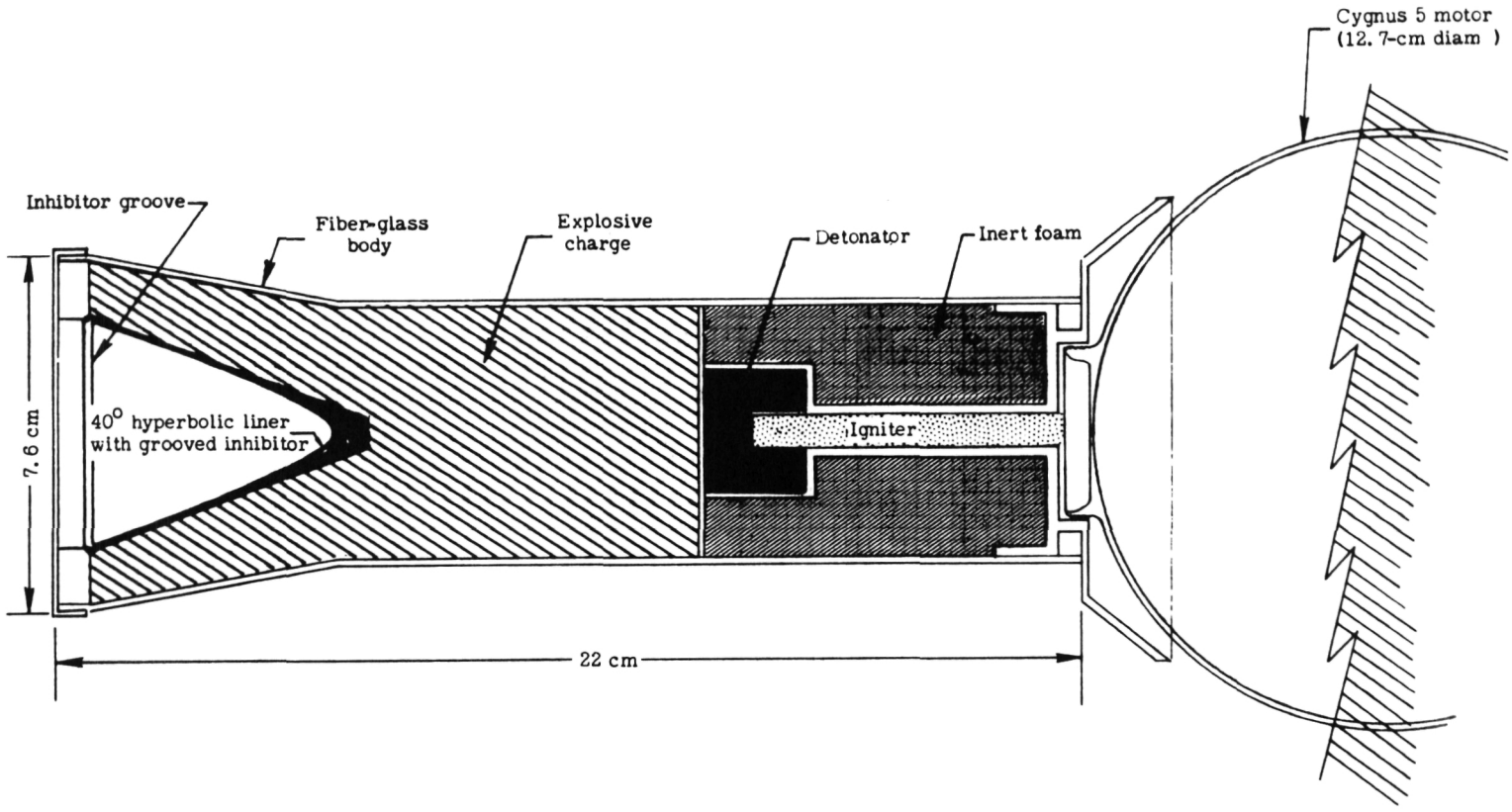

Figure 7.- Shaped charge accelerator used in two experiments.

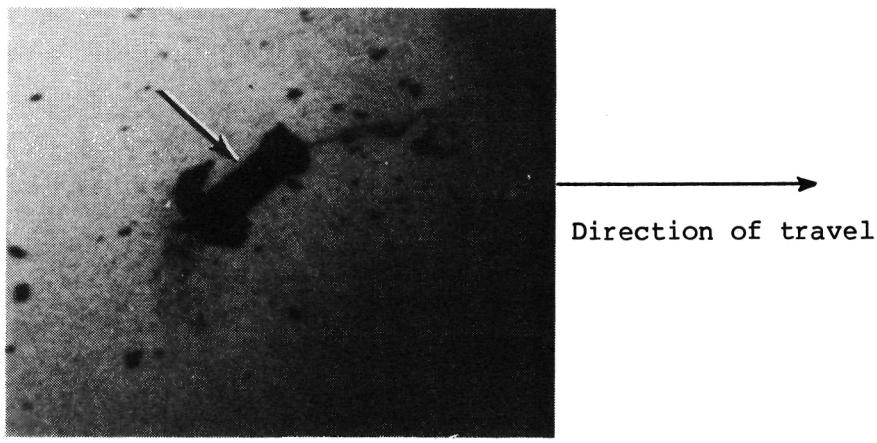

L-78-157

Figure 8.- Flash radiograph of nickel pellet formed in ground tests of shaped charge accelerators.

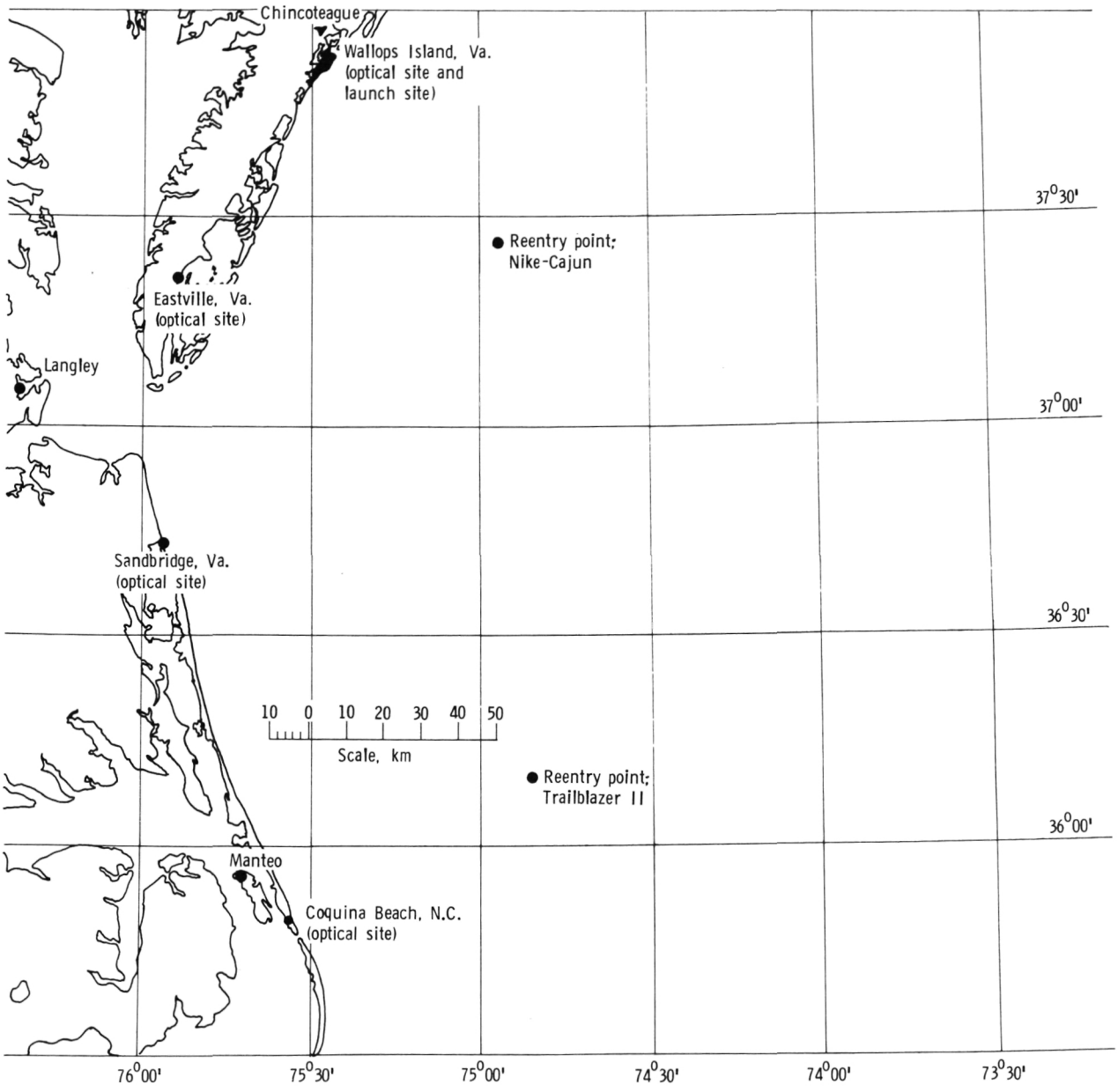

Figure 9.- Locations of camera sites with respect to reentry area.

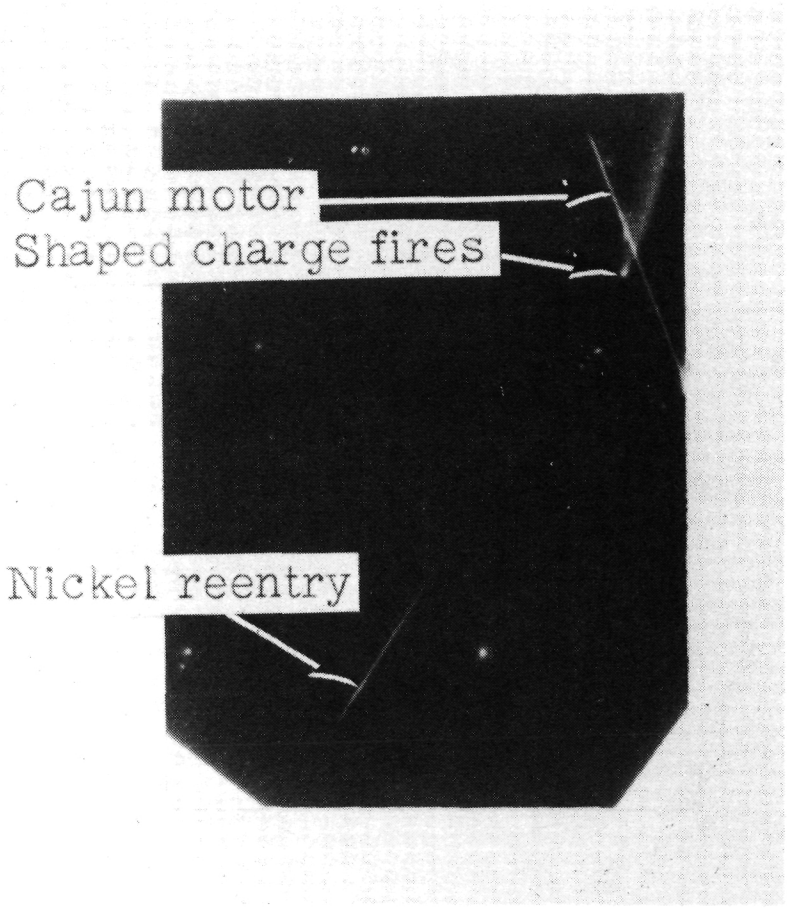

L-78-158

Figure 10.- Super-Schmidt photograph of meteor 1.

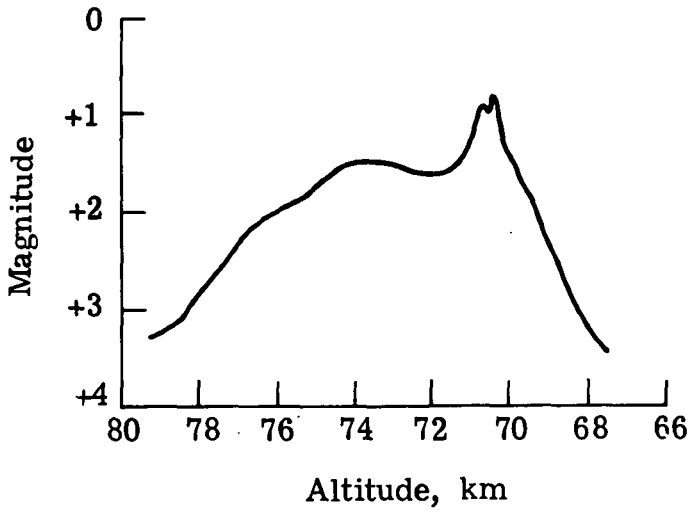

(a) Meteor 1.

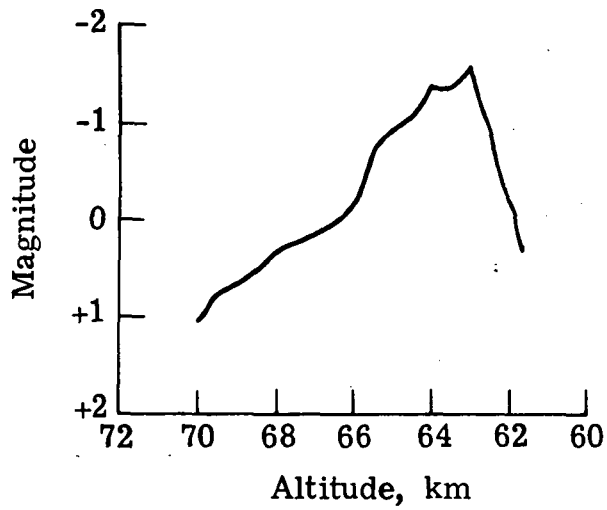

(b) Meteor 2.

Figure 11.- Light-intensity curves for four artificial meteors.

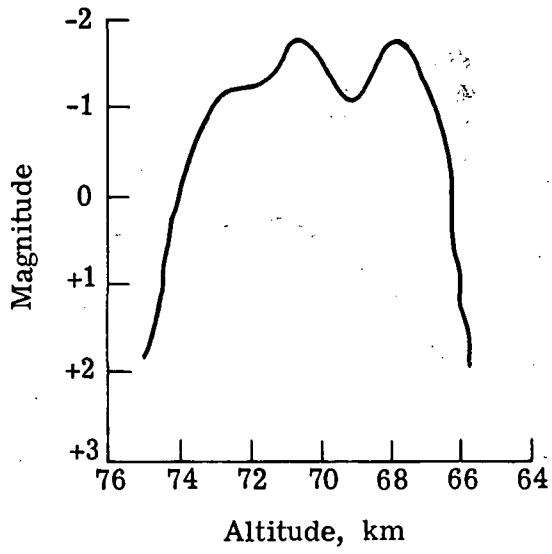

(c) Meteor 3.

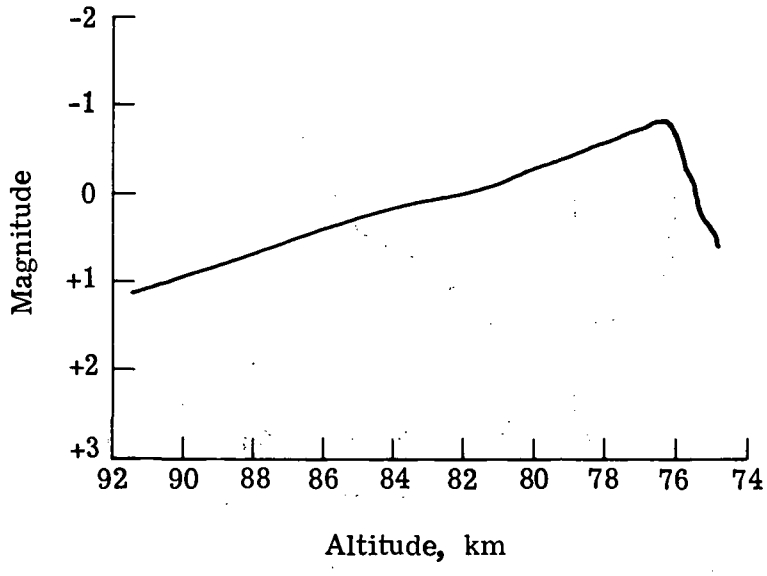

(d) Meteor 4.

Figure 11.- Concluded.

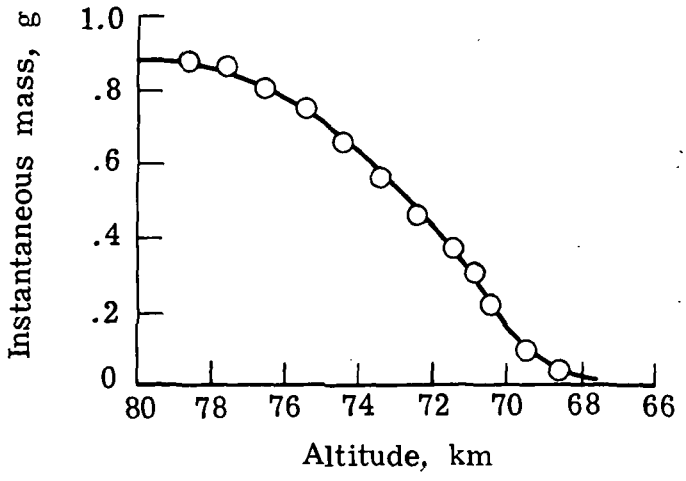

(a) Meteor 1.

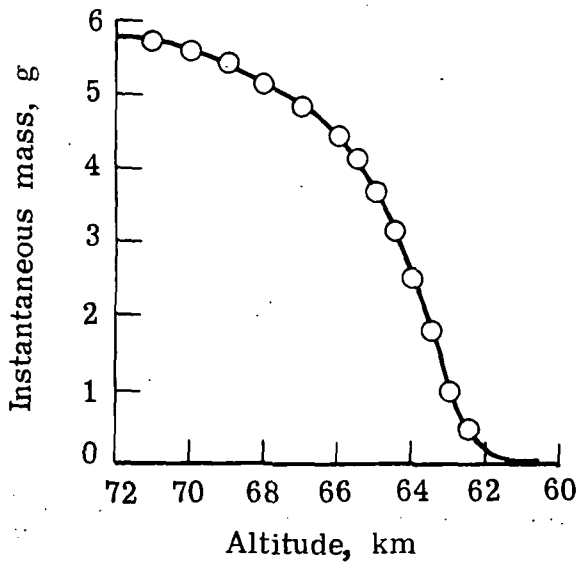

(b) Meteor 2.

Figure 12.- Mass-loss curves for four artificial meteoroids.

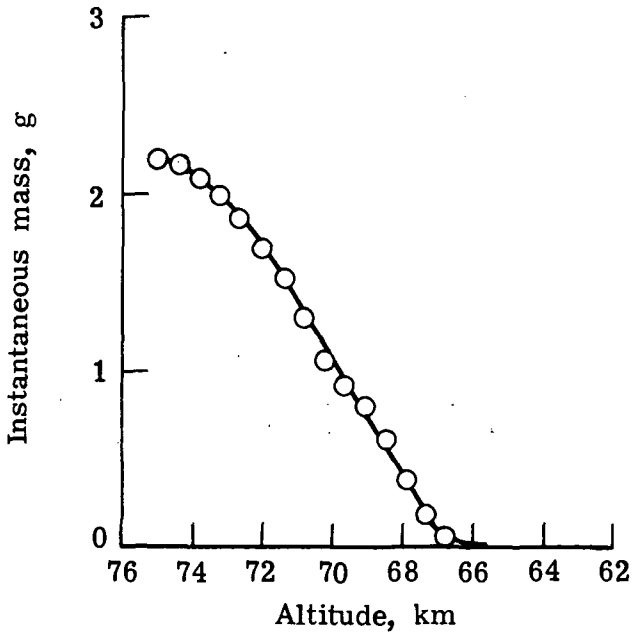

(c) Meteor 3.

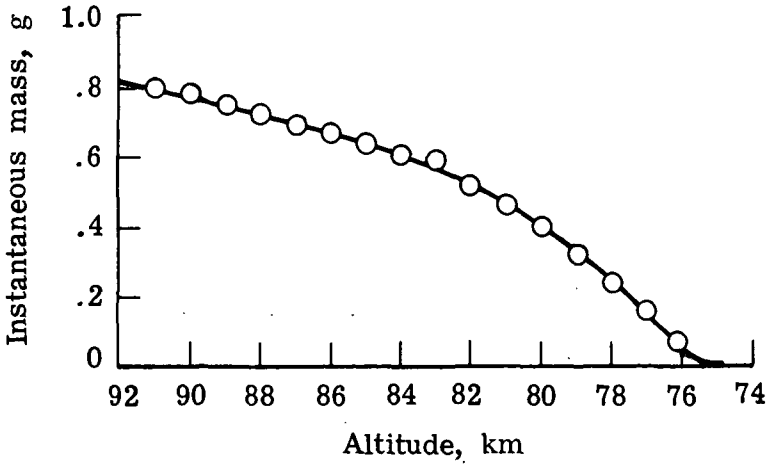

(d) Meteor 4.

Figure 12.- Concluded.

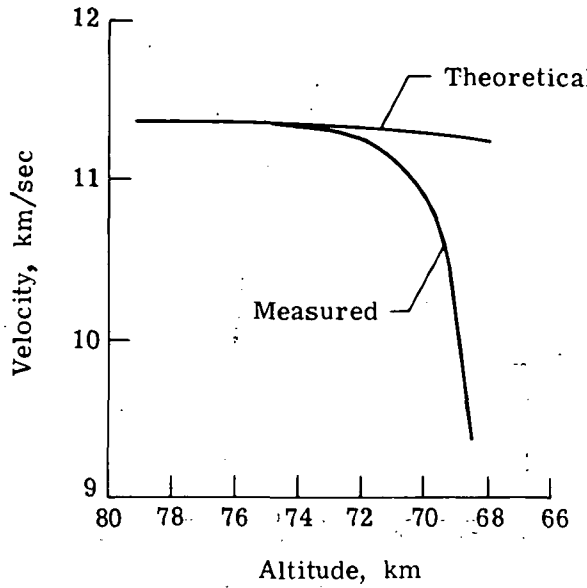

(a) Meteor 1.

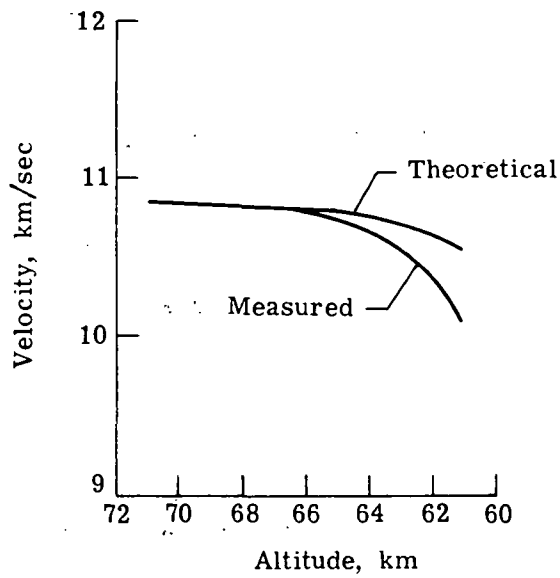

(b) Meteor 2.

Figure 13.- Comparison of theoretical velocity-altitude curves for nonfragmenting meteoroids to their measured (observationally determined) velocity-altitude curves.

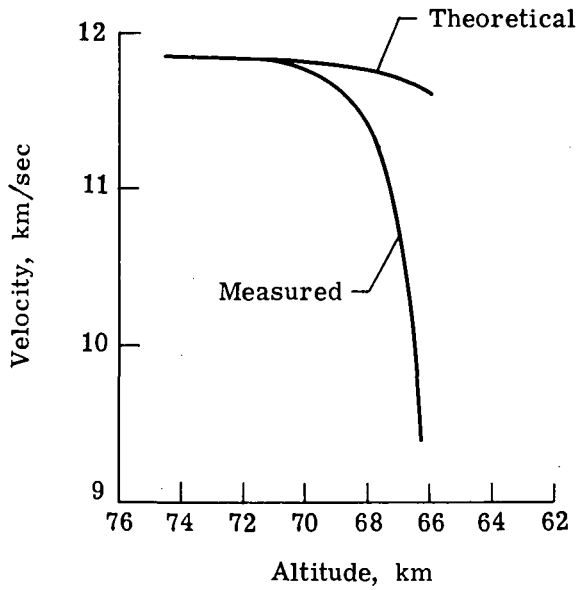

(c) Meteor 3.

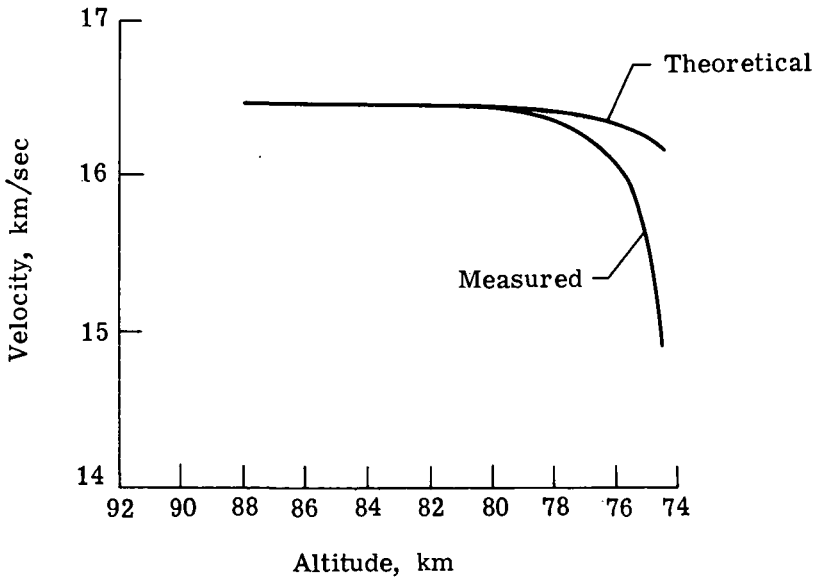

(d) Meteor 4.

Figure 13.- Concluded.

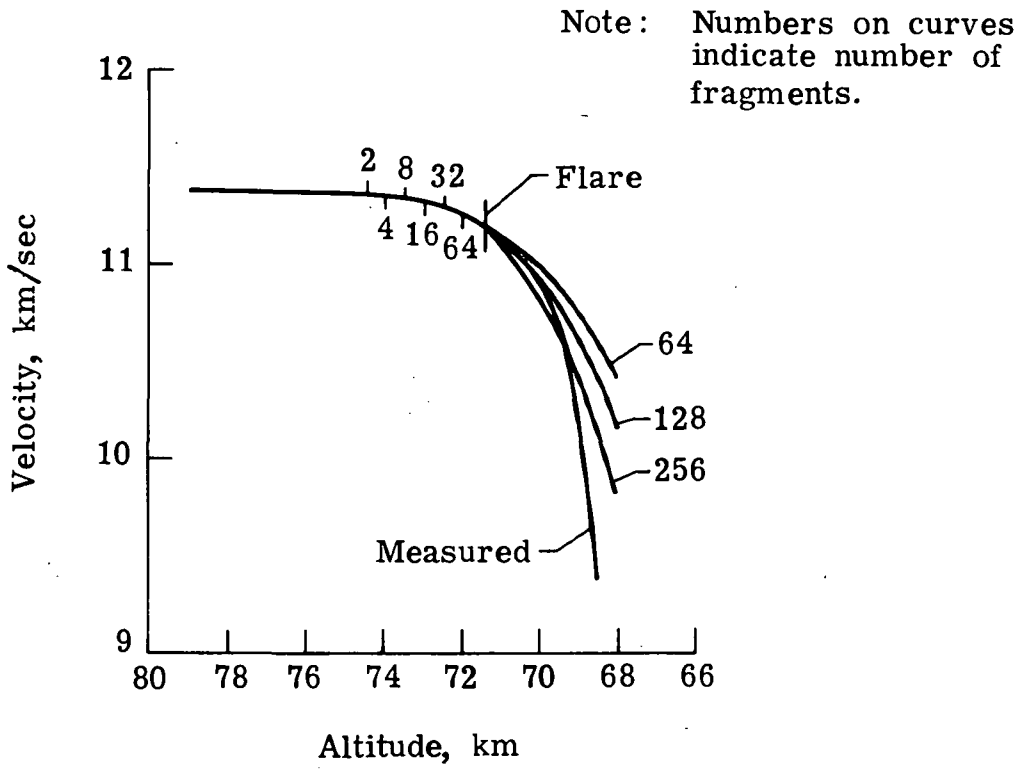

(a) Meteor 1.

Figure 14.- Comparison of theoretical velocity-altitude curves to their measured velocity-altitude curves for four artificial meteoroids, taking fragmentation into account.

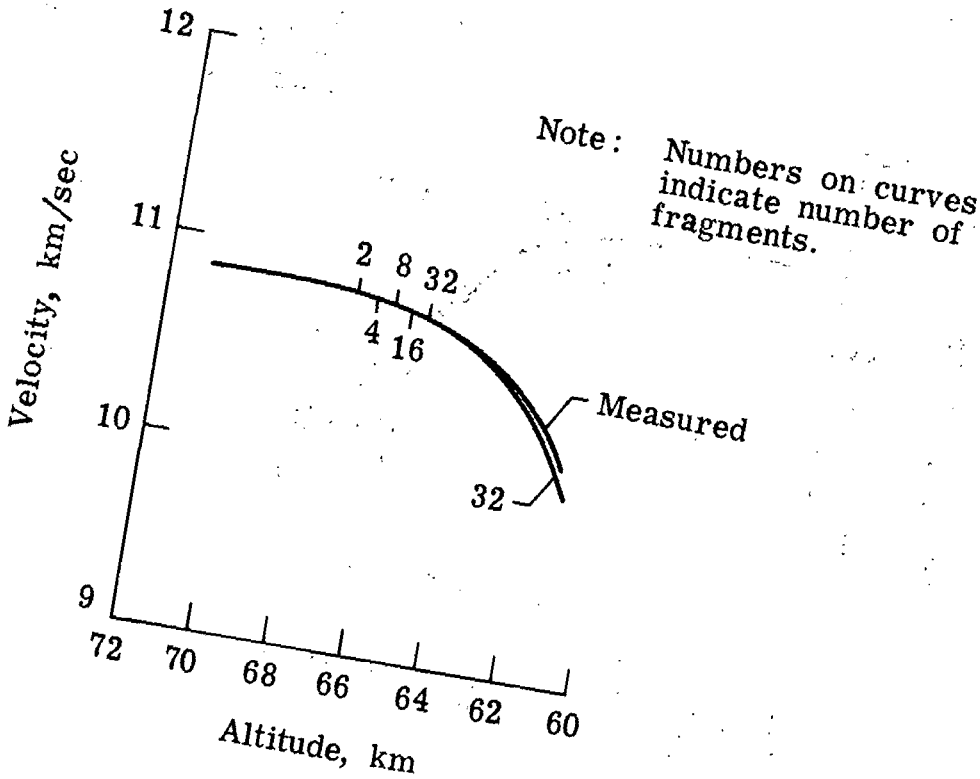

(b) Meteor 2.

Figure 14.- Continued.

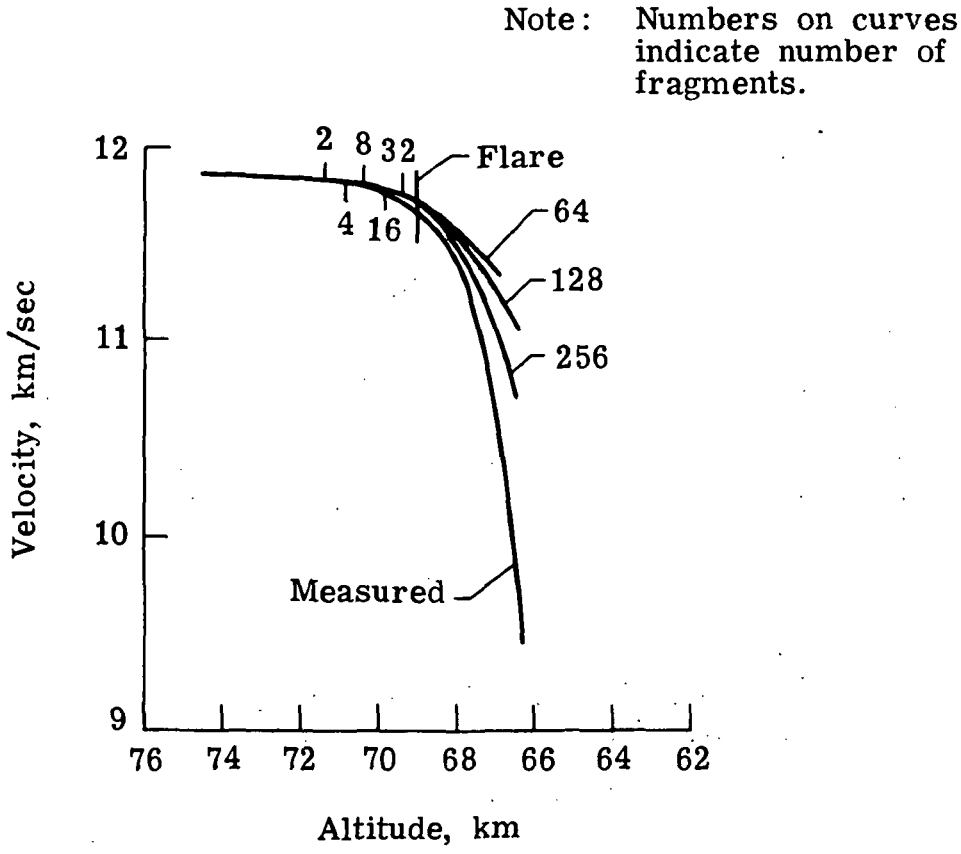

(c) Meteor 3.

Figure 14.- Continued.

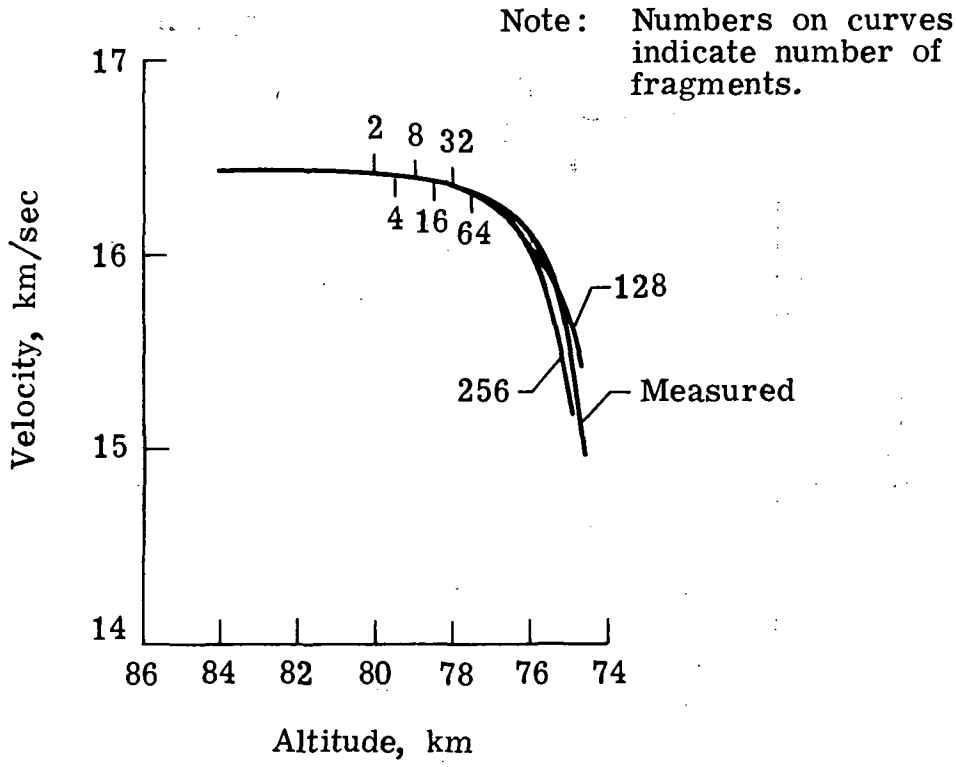

(d) Meteor 4.

Figure 14.- Concluded.

1. Report No.	2. Government Accession No.	3. Recipient's Catalog No.
NASA TP-1333		

4. Title and Subtitle	5. Report Date
ATMOSPHERIC ENTRY AND FRAGMENTATION OF DENSE METEOROIDS	January 1979
	6. Performing Organization Code

7. Author(s)	8. Performing Organization Report No.
T. Dale Bess	L-12508
	10. Work Unit No. 175-40-30-02

9. Performing Organization Name and Address	11. Contract or Grant No.
NASA Langley Research Center Hampton, VA 23665	

12. Sponsoring Agency Name and Address	13. Type of Report and Period Covered
National Aeronautics and Space Administration Washington, DC 20546	Technical Paper
	14. Sponsoring Agency Code

15. Supplementary Notes

16. Abstract

Fragmentation characteristics for four artificial meteoroids of high density and high tensile strength with varying size, velocity, and material are investigated. The meteoroids analyzed were lifted to natural meteor altitude by a rocket vehicle system. The meteoroids were then accelerated back into the Earth's atmosphere at natural meteor velocities. This paper investigates anomalous deceleration of high-density meteors and shows that anomalies in the deceleration are due to progressive fragmentation of the meteoroids. These anomalies in the deceleration of high-density meteoroids are similar to the anomalies that occur in the deceleration of natural meteors, which are generally assumed to be porous and of weak structure.

17. Key Words (Suggested by Author(s))	18. Distribution Statement
Meteoroid Meteor Deceleration Fragmentation Atmospheric entry Luminous efficiency	Unclassified - Unlimited Subject Category 91

19. Security Classif. (of this report)	20. Security Classif. (of this page)	21. No. of Pages	22. Price*
Unclassified	Unclassified	34	$4.50

* For sale by the National Technical Information Service, Springfield, Virginia 22161

NASA-Langley, 1979

National Aeronautics and
Space Administration

Washington, D.C.
20546

Official Business
Penalty for Private Use, $300

THIRD-CLASS BULK RATE

Postage and Fees Paid
National Aeronautics and
Space Administration
NASA-451

NASA

POSTMASTER: If Undeliverable (Section 158 Postal Manual) Do Not Return